The Astrophysical Journal, 847:68 (5pp), 2017 September 20 https://doi.org/10.3847/1538-4357/aa87b7

The Orbit of the Gamma-Ray Binary 1FGL J1018.6−5856

I. M. Monageng[1,2], V. A. McBride[1,2,3], L. J. Townsend[2], A. Y. Kniazev[1,5,6,7], S. Mohamed[1,2,8], and M. Böttcher[4]
[1] South African Astronomical Observatory, P.O Box 9, Observatory, 7935, Cape Town, South Africa
[2] Department of Astronomy, University of Cape Town, Private Bag X3, Rondebosch 7701, South Africa
[3] Office of Astronomy for Development, IAU, Cape Town, South Africa
[4] Centre for Space Research, North-West University, Potchefstroom, 2531, South Africa
[5] Southern African Large Telescope Foundation, P.O. Box 9, Observatory, 7935, Cape Town, South Africa
[6] Sternberg Astronomical Institute, Lomonosov Moscow State University, Universitetskij Pr. 13, Moscow 119992, Russia
[7] Special Astrophysical Observatory of RAS, Nizhnij Arkhyz, Karachai-Circassia 369167, Russia
[8] South Africa National Institute for Theoretical Physics, Private Bag X1, Matieland, 7602, South Africa
Received 2017 July 7; revised 2017 August 17; accepted 2017 August 20; published 2017 September 21

Abstract

Gamma-ray binaries are a small subclass of the high mass X-ray binary population that exhibit emission across the whole electromagnetic spectrum. We present the radial velocities of 1FGL J1018.6−5856 based on the observations obtained with the Southern African Large Telescope. We combine our measurements with those published in the literature to get a broad phase coverage. The mass function obtained supports a neutron star compact object, although a black hole mass is possible for the very low inclination angles. The improved phase coverage allows constraints to be placed on the orbital eccentricity ($e = 0.31 \pm 0.16$), which agrees with the estimates from the high-energy data.

Key words: binaries: spectroscopic – stars: massive – stars: neutron

1. Introduction

Gamma-ray binaries (GRBis) are a small subclass of high mass X-ray binaries (HMXBs), comprising of only six sources: PSR B1259−63 (Johnston et al. 1992), LS 5039 (Motch et al. 1997), LS I+61 303 (Gregory & Taylor 1978), HESS J0632+057 (Aharonian et al. 2007), 1FGL J1018.6−5856 (Fermi LAT Collaboration et al. 2011), and LMC P3 (Corbet et al. 2016). These systems comprise of a pulsar or a black hole (BH) and a massive O or Be star. GRBis differ from traditional HMXBs (Be X-ray and supergiant X-ray binaries) in that they show a peak in their spectral energy distribution (SED) above 1 MeV, as well as display multiwavelength emission across the whole electromagnetic spectrum. In all but one case (PSR B1259−63) the nature of the compact object is uncertain (it is either a neutron star or a BH). Through radio pulse timing, a pulse period of 47.7 ms was found in PSR B1259−63, confirming the nature of the compact object as a pulsar. Pulsations are not detected in any of the other gamma-ray binaries. Furthermore, the large uncertainty in the mass function results in a large uncertainty in the calculated mass of the compact object in the other systems, making it difficult to distinguish between a pulsar and a BH (a minimum compact object mass of 3 $M_{\odot}$ would indicate a BH).

1FGL J1018.6−5856 (J1018), the subject of this paper, was discovered at GeV energies when a 16.6 day modulation was detected from the first *Fermi*/LAT catalog (Fermi LAT Collaboration et al. 2011). Follow-up work at optical wavelengths taken with the 1.9 m telescope at the South African Astronomical Observatory and the 2.5 m telescope at Las Campanas Observatory revealed Balmer, He I, and He II absorption lines (similar to LS 5039), with the He II/He I ratio indicating an O6V((f)) spectral type (Fermi LAT Collaboration et al. 2012).

Using Échelle spectra obtained with the CTIO 1.5 m telescope, Waisberg & Romani (2015b) performed a radial velocity (RV) analysis of J1018. Using Gaussian fits to the H I, He I, and He II absorption lines, Waisberg & Romani (2015b) found a semi-amplitude (K) range of 12−40 km s^{-1}. The maximum determined semi-amplitude (40 km s^{-1}) from their work indicates that the compact object likely has a mass >2.2 $M_{\odot}$, favoring a BH. The RV curve from Waisberg & Romani (2015b), however, is hindered by a large scatter due to the imprecision of the continuum calibration, as well as possible contamination by stellar wind line features. Strader et al. (2015; S15) performed a follow-up RV study of J1018 using medium resolution (MR) spectra obtained with the Goodman High-Throughput Spectrograph onboard the SOAR 4.1 m telescope. They performed a cross-correlation of their spectra against the O6V star, HD 172275, in two wavelength regions with the Hγ line and He II lines (4542 and 4686 Å). The two RV plots show different systemic velocities, with the He II RV measurements offset from the Balmer line measurements by +6 km s^{-1}. A similar behavior from those of the RV measurements made from the two line species has been reported in LS 5039, which is believed to be due to the contamination of wind for the He II and H I (Casares et al. 2005; Sarty et al. 2011). With a modest phase coverage, S15 performed a circular Keplerian fit to the RV measurements and found semi-amplitudes of 11.4 ± 1.5 km s^{-1} and 12.2 ± 2.7 km s^{-1} from Hγ and He II, respectively. S15 found that for inclination angles between 26° and 64°, a compact object mass of 1.4−2.5 $M_{\odot}$ (canonical neutron star mass range) is obtained, while for lower inclination angles $i \leqslant 16°$) a BH is favored ($M_X \geqslant 5\,M_{\odot}$).

In this work, we present new Échelle optical spectroscopy of J1018 obtained with the High Resolution Spectrograph (HRS) on the Southern African Large Telescope (SALT). The broader phase coverage, combined with radial velocities from S15, allows for better constraints on the orbital parameters and hence a better mass estimate of the compact object.

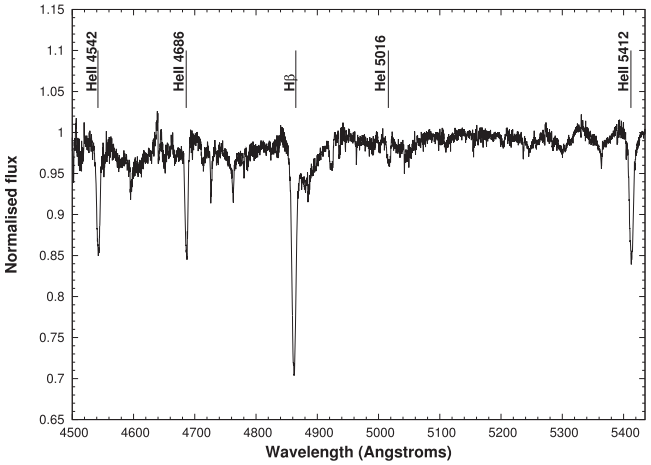

Figure 1. Normalized average blue spectrum for the wavelength range used for 1FGL J1018.6−5856 with the strongest lines used for the cross-correlation labeled.

2. Observations and Reductions

J1018 was observed eight times with SALT (Buckley et al. 2006) using the HRS (Bramall et al. 2010, 2012; Crause et al. 2014) between 2015 December 06 and 20. Our observations were done in the MR mode ($R \sim 40{,}000$) with the blue and red arms, providing a total wavelength coverage of ∼3700−8900 Å. Only spectra with wavelength ranges 4500 −5500 Å and 5700−6750 Å for the blue and red arms, respectively, were usable. All observations were performed with exposure times of 1400 s. Regular calibration sets of ThAr arc lamps, bias, and flats were taken throughout the duration of our program. Primary reductions of the spectra (including overscan correction, bias subtraction, and gain correction) were performed with the SALT science pipeline (Crawford 2015). The subsequent reduction steps, which include background subtraction, removal of the blaze function, identification of the arc lines, and merging of the orders for the object spectra were carried out using the MIDAS FEROS (Stahl et al. 1999) and ECHELLE (Ballester 1992) packages (see Kniazev et al. 2016 for a detailed description of the reduction steps). The spectra were normalized and corrected for the heliocenter using the IRAF[9] tasks RVCORRECT and DOPCOR.

3. Radial Velocities

For our analysis we use the blue spectra to measure the radial velocities. Figure 1 shows the mean spectrum of J1018 with the strongest absorption lines of He I (5016 Å), He II (4542, 4686, and 5411 Å), and Hβ present. For the wavelength range that we have access to, the mean spectrum is consistent with that of the low resolution spectrum of Fermi LAT Collaboration et al. (2012). To obtain the radial velocities we performed a cross-correlation using the blue arm spectra. We used an iterative process described by Manick et al. (2015) and Foellmi et al. (2003) to generate a high signal-to-noise ratio (S/N) zero velocity template. First, individual spectra were rectified and the continuum level was subtracted. Each spectrum was then converted to a logarithmic wavelength scale and the spectra were grouped according to their S/N (highest to lowest). The RV shifts of each spectrum relative to the spectrum with the highest S/N were measured. Individual spectra were then shifted to the same rest wavelength as the high S/N template using the results of the first cross-correlation iteration, and a mean spectrum created by combining all of the shifted spectra. This became our final template spectrum, which was then used to compute the RV shifts. These shifts (converted to velocities) are shown in Table 1 and Figure 2 (filled circles).

Different combinations of the line species were considered during the cross-correlation analysis, however no significant differences in the RV amplitudes were found. The final values of RV used are those from all of the available lines in the wavelength range of 4500−5500 Å. The measurements obtained from this work are combined with those from S15. S15 consider the two line species of He II (4542 and 4686 Å) and Hβ separately. Previous RV studies involving O stars have considered the two line species separately (Casares et al. 2005; Sarty et al. 2011) in the case of LS 5039. The Balmer lines are more contaminated by the wind emission than by the He II lines, which originate from the stellar photosphere (Puls et al. 1996; Sarty et al. 2011; Waisberg & Romani 2015a), making He II lines more reliable in the derivation of the orbital parameters. For the reasons explained above, we use the combined RV values from our work using the full wavelength range of the blue spectra and the He II measurements from S15 to derive the final orbital solutions. A Keplerian model (Figure 2) was fitted to the combined measurements with the period fixed to that derived from the X-ray studies of J1018 ($P = 16.544$ days; An et al. 2015). We used the RVLIN software package provided by Wright & Howard (2009) to perform the Keplerian fits and to obtain the model parameters. The uncertainties in the best-fit parameters were obtained using

Table 1
Radial Velocities of 1FGL J1018.6−5856 from SALT

BJD (days)	Velocity (km s^{-1})
2457362.5348	31.4 ± 3.6
2457363.5595	36.9 ± 4.9
2457365.5589	37.9 ± 4.2
2457367.5202	44.4 ± 3.4
2457371.5214	40.9 ± 3.3
2457373.5396	31.6 ± 6.0
2457375.5024	22.9 ± 3.9
2457377.4990	19.5 ± 10.9

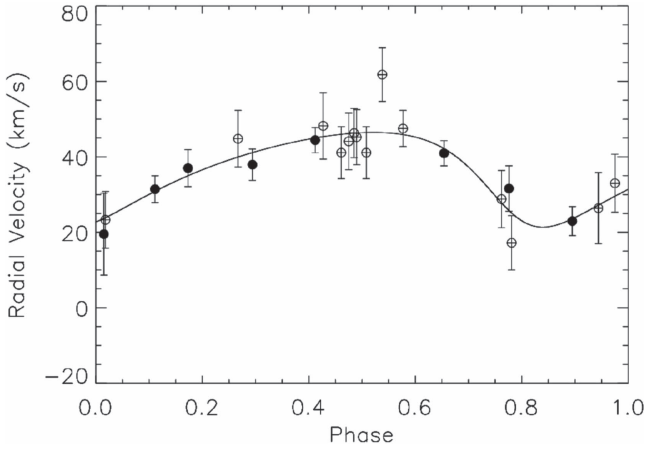

Figure 2. Best-fitting curve to the radial velocities of the He II lines. The unfilled circles are from Strader et al. (2015) and the filled circles are from this work.

[9] Image Reduction and Analysis Facility: iraf.noao.edu.

Table 2
Orbital Elements of 1FGL J1018.6−5856

Parameter	Value
P_{orb} (days)	16.544 (fixed)
T_p (JD)	2457256.0 ± 1.2
e	0.31 ± 0.16
$\omega(^\circ)$	89 ± 30
K (km s^{-1})	12.3 ± 1.9
γ (km s^{-1})	35.5 ± 1.3
rms of fit (km s^{-1})	5.85

the BOOTTRAN bootstrapping routines described in Wang et al. (2012). We note that if the period is left as a free parameter, a period of $P = 16.583 \pm 0.042$ days is derived, which is in good agreement with the X-ray period (as well as that derived from the gamma-rays, $P = 16.549 \pm 0.007$ days; Coley et al. 2014). A summary of the orbital parameters is presented in Table 2.

4. Mass of the Compact Object

The derived orbital parameters allow us to use the mass function defined by

$$f(M_x) = \frac{PK^3}{2\pi G}(1 - e^2)^{3/2} = \frac{(M_x \sin i)^3}{(M_x + M_O)^2}, \quad (1)$$

where M_x and M_O are the masses of the compact object and optical companion, respectively, and i is the inclination angle of the orbit. For the remainder of the analysis, we use an optical companion mass range for an O6V((f)) of 20−26.4 $M_\odot$ as used by Casares et al. (2005), Strader et al. (2015), and Waisberg & Romani (2015b). For the parameters listed in Table 2 a mass function of $f(M_x) = 0.0027 \pm 0.0013$ $M_\odot$ is obtained. From this, the mass of the compact object can be calculated for different inclination angles. Figure 3 shows the mass–mass plot obtained from the orbital parameters derived from the RV fit. Referring to Figure 3 for a lower limit mass of the optical companion (20 $M_\odot$) and a canonical neutron star mass range of 1.4−2.5 $M_\odot$ implies an orbital inclination angle range of ∼50°–26°. For the upper limit optical companion mass of 26.4 $M_\odot$, inclination angles between ∼70° and 32° are implied. The most massive neutron star (NS) known has a mass of 2.0 $M_\odot$ (Antoniadis et al. 2013), which corresponds to inclination angles of $i = 33^\circ$ and $i = 41^\circ$ for optical companion masses of 20 $M_\odot$ and 26.4 $M_\odot$, respectively. For the compact object to be a BH ($M_x \geqslant 3.0$ $M_\odot$), lower inclination angles of $i < 22^\circ$ and $i < 26^\circ$ for optical companion masses of 20 $M_\odot$ and 26.4 $M_\odot$, respectively, are implied.

5. Discussion

The value of the mass function obtained from this study agrees with that found by Strader et al. (2015) within the errors. For the mass range of the companion star considered, we also find similar values for the allowed inclination angles for the different masses of the compact object (Figure 3). We obtained a best-fit Keplerian model of eccentricity $e = 0.31 \pm 0.16$. The probability of this model, given our data, is $P(\chi^2 > 11.05) \sim 85\%$ (a circular fit results in a probability of ∼50%). The analysis of *Fermi* GeV data revealed a relatively low modulation amplitude which, if the gamma-ray flux is due to anisotropic inverse Compton scattering of stellar photons by energetic electrons, implies low inclination and eccentricity (Chen et al. 2017). An & Romani (2017) model the X-ray and gamma-ray light curves and SED of J1018, where the fit of the model to the spike in the modulated X-ray light curve is explained by an orbital eccentricity of $e = 0.35$ and an inclination angle of $i \sim 50^\circ$. These implications for the inclination angle from the high-energy analysis further support a NS as the compact object in J1018. Furthermore, the mass of the donor star could be significantly less than those of the estimates used, which is typical of donors in HMXBs to display different characteristics than those of a main-sequence equivalent (e.g., Coe et al. 2015; Rajoelimanana et al. 2017 and references therein). This would reduce the mass estimate of the compact object for a given mass function, making a NS even more likely. The wide phase coverage allows us to put constraints on the orbital eccentricity, which is also in agreement (within the errors) with estimates from the high-energy studies (An & Romani 2017). Figure 4 shows the orbit of the

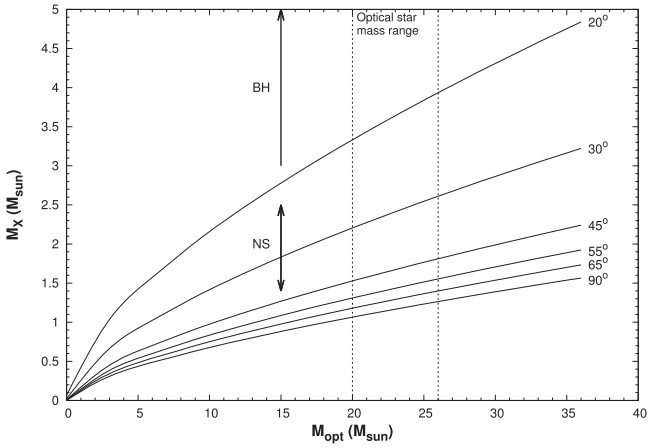

Figure 3. Mass constraints for the two systems in 1FGL J1018.6−5856 for the different inclination angles. The two vertical lines show the mass range for the optical star.

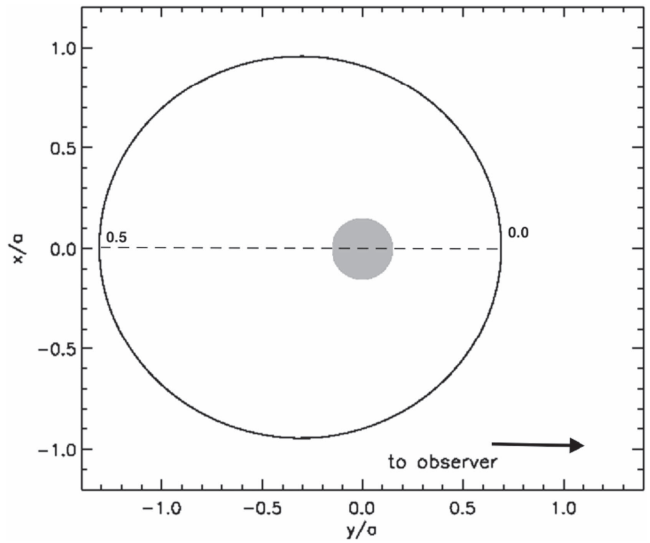

Figure 4. Orbit of the compact object around the optical companion (shaded circle) in J1018 as seen from above the orbital plane. Periastron and apastron phases are indicated in the plot. The coordinates are in units of the semimajor axis.

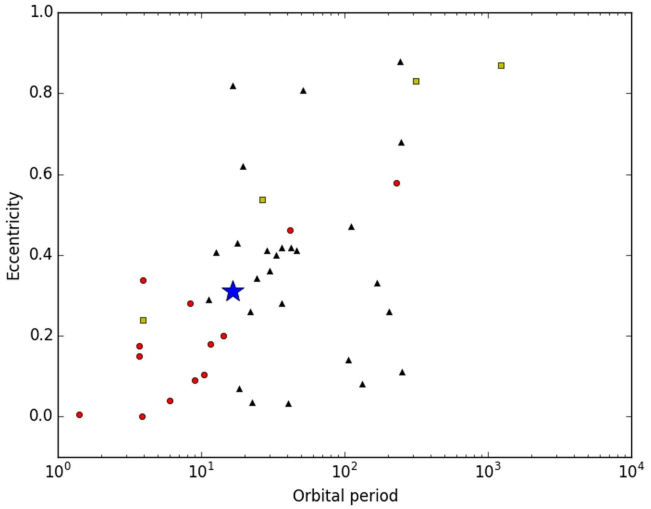

Figure 5. Updated orbital period against eccentricity for HMXBs from Townsend et al. (2011). The red circle, black triangle, and yellow square symbols represent supergiant, Be X-ray, and GRBi systems, respectively. The blue star represents J1018.

compact object around the optical companion as viewed from an inclination angle of $i = 0°$. This was produced using a mass and radius of 22.9 $M_\odot$ and 9.3 $R_\odot$, respectively, for the optical companion (Casares et al. 2005) and a compact object of mass of 1.4 $M_\odot$. From Figure 4, the periastron passage of the compact object occurs close to inferior conjunction (INFC). The peak of the X-ray, GeV, and TeV emission in J1018 occurs at similar phases (An et al. 2015; H. E. S. S. Collaboration et al. 2015). If the gamma-ray emission is due to anisotropic inverse Compton scattering of stellar photons, then the GeV peak is expected to occur at phases when the compact object is behind the donor star (superior conjunction; SUPC), while the TeV emission is expected to be at the maximum at INFC (since absorption is at the maximum at SUPC). The peculiar behavior of the emission maxima resulting at similar phases is discussed by S15, where a proposed solution is the occurrence of INFC and periastron passage at a similar phase.

Figure 5 shows the updated orbital period versus eccentricity plot from Townsend et al. (2011) for HMXBs with J1018 included from the derived orbital eccentricity in this work. J1018 lies around the transition zone between supergiant and Be X-ray binary systems, and follows the correlation of the two quantities that was noted by Casares et al. (2012) for the GRBis with known orbital parameters. It was speculated that the correlation between the eccentricity and the orbital period in GRBis is due to the small separation required for very high-energy (TeV) emission to be triggered, which for long period systems requires large eccentricities. With the limited sample, GRBis display the same characteristics as those of accreting HMXBs, supporting the notion that GRBis may represent an earlier phase in the evolution of HMXBs.

6. Conclusion

We observed J1018 with SALT and, combining our observations with S15, we obtain orbital phase coverage that allows us to constrain the orbital parameters. In particular, we obtained an eccentricity of $e = 0.31 \pm 0.16$ and a mass function of $f(M_x) = 0.0027 \pm 0.0013\ M_\odot$. The eccentricity obtained is in agreement with that implied from high-energy studies of the source. For a range of values of the mass of the optical companion of 20–26.4 $M_\odot$, the mass function obtained gives a mass for the compact object which favors a NS, with a BH possible for very low inclination angles ($i \lesssim 26°$).

We thank the anonymous referee for helpful comments that improved the paper. All spectral observations reported in this paper were obtained with the South African Large Large Telescope under the proposal code 2015-2-SCI-045 (PI: Monageng). We thank Brent Miszalski and Yuki Moritani for the useful discussions related to the cross-correlation techniques. I.M. acknowledges funding from the UCT science faculty PhD fellowship. V.M. acknowledges support of the National Research Foundation of South Africa (Grant nos. 98969 and 93405). A.K. acknowledges the National Research Foundation of South Africa and the Russian Science Foundation (project no. 14-50-00043). S.M. is grateful to the South African National Research Foundation (NRF) for a research grant. The work of M.B. is supported by the South African Department of Science and Technology and National Research Foundation through the South African Research Chairs Initiative.

Software: SALT science pipeline (Crawford 2015), Feros (Stahl et al. 1999), echelle (Ballester 1992), IRAF (Tody 1986, 1993), rvlin (Wright & Howard 2009), boottran (Wang et al. 2012).

ORCID iDs

I. M. Monageng https://orcid.org/0000-0002-4754-3526
A. Y. Kniazev https://orcid.org/0000-0001-8646-0419
M. Böttcher https://orcid.org/0000-0002-8434-5692

References

Aharonian, F. A., Akhperjanian, A. G., Bazer-Bachi, A. R., et al. 2007, A&A, 469, L1
An, H., Bellm, E., Bhalerao, V., et al. 2015, ApJ, 806, 166
An, H., & Romani, R. W. 2017, ApJ, 838, 145
Antoniadis, J., Freire, P. C. C., Wex, N., et al. 2013, Sci, 340, 448
Ballester, P. 1992, in ESO Conf. and Workshop Proc. 41, ed. P. J. Grosbøl & R. C. E. de Ruijsscher (Munich: ESO), 77
Bramall, D. G., Schmoll, J., Tyas, L. M. G., et al. 2012, Proc. SPIE, 8446, 84460A
Bramall, D. G., Sharples, R., Tyas, L., et al. 2010, Proc. SPIE, 7735, 77354F
Buckley, D. A. H., Charles, P. A., Nordsieck, K. H., & O'Donoghue, D. 2006, in IAU Symp. 232, The Scientific Requirements for Extremely Large Telescopes, ed. P. Whitelock, M. Dennefeld, & B. Leibundgut (Cambridge: Cambridge Univ. Press), 1
Casares, J., Ribó, M., Ribas, I., et al. 2005, MNRAS, 364, 899
Casares, J., Ribó, M., Ribas, I., et al. 2012, MNRAS, 421, 1103
Chen, A. M., Ng, C. W., Takata, J., Yu, Y. W., & Cheng, K. S. 2017, arXiv:1703.08080
Coe, M. J., Bartlett, E. S., Bird, A. J., et al. 2015, MNRAS, 447, 2387
Coley, J. B., Corbet, R., Cheung, C. C., et al. 2014, in AAS Meeting #14, 122.10
Corbet, R. H. D., Chomiuk, L., Coe, M. J., et al. 2016, ApJ, 829, 105
Crause, L. A., Sharples, R. M., Bramall, D. G., et al. 2014, Proc. SPIE, 9147, 91476T
Crawford, S. M. 2015, pyhrs: Spectroscopic data reduction package for SALT, Astrophysics Source Code Library, ascl:1511.005
Fermi LAT Collaboration, Ackermann, M., Ajello, M., et al. 2012, Sci, 335, 189
Fermi LAT Collaboration, Corbet, R. H. D., Coe, M. J., et al. 2011, in AAS Meeting #12, 3.07
Foellmi, C., Moffat, A. F. J., & Guerrero, M. A. 2003, MNRAS, 338, 360
Gregory, P. C., & Taylor, R. 1978, IAUC, 3164, 1
H. E. S. S. Collaboration, Abramowski, A., Aharonian, F., et al. 2015, A&A, 577, A131

Johnston, S., Lyne, A. G., Manchester, R. N., et al. 1992, MNRAS, 255, 401
Kniazev, A. Y., Gvaramadze, V. V., & Berdnikov, L. N. 2016, MNRAS, 459, 3068
Manick, R., Miszalski, B., & McBride, V. 2015, MNRAS, 448, 1789
Motch, C., Haberl, F., Dennerl, K., Pakull, M., & Janot-Pacheco, E. 1997, A&A, 323, 853
Puls, J., Kudritzki, R.-P., Herrero, A., et al. 1996, A&A, 305, 171
Rajoelimanana, A. F., Charles, P. A., Meintjes, P. J., et al. 2017, MNRAS, 464, 4133
Sarty, G. E., Szalai, T., Kiss, L. L., et al. 2011, MNRAS, 411, 1293
Stahl, O., Kaufer, A., & Tubbesing, S. 1999, in ASP Conf. Ser. 188, Optical and Infrared Spectroscopy of Circumstellar Matter, ed. E. Guenther, B. Stecklum, & S. Klose (San Francisco, CA: ASP), 331
Strader, J., Chomiuk, L., Cheung, C. C., Salinas, R., & Peacock, M. 2015, ApJL, 813, L26
Tody, D. 1986, Proc. SPIE, 627, 733
Tody, D. 1993, in ASP Conf. Ser. 52, Astronomical Data Analysis Software and Systems II, ed. R. J. Hanisch, R. J. V. Brissenden, & J. Barnes (San Francisco, CA: ASP), 173
Townsend, L. J., Coe, M. J., Corbet, R. H. D., & Hill, A. B. 2011, MNRAS, 416, 1556
Waisberg, I. R., & Romani, R. W. 2015a, ApJ, 805, 18
Waisberg, I. R., & Romani, R. W. 2015b, ApJ, 812, 178
Wang, X. S., Wright, J. T., Cochran, W., et al. 2012, ApJ, 761, 46
Wright, J. T., & Howard, A. W. 2009, ApJS, 182, 205